Electrophoresis 2019, *40*, 1230–1244

Feifei Tan
Tianbao Wang
Haishi Wang
Yuzheng Zheng

College of Communication Engineering, Chengdu University of Information Technology, Chengdu, Sichuan, P. R. China

Received September 30, 2018
Revised November 20, 2018
Accepted December 2, 2018

Review

Microfluidic techniques for tumor cell detection

Cancer metastasis is the main cause of cancer-related death. Early detection of tumor cell in peripheral blood is of great significant to early diagnosis and effective treatment of cancer. Over the past two decades, microfluidic technologies have been demonstrated to have great potential for isolating and detecting tumor cell from blood. The present paper reviews microfluidic techniques for tumor cell detection based on various physical principles. The specific methods are categorized into active and passive methods depending on whether extra force field is applied. Working principles of the two methods are explained in detail, including microfluidics combined with optical tweezer, electric field, magnetic field, acoustophoresis, and without extra fields for tumor cell detection. Typical experiments and the results are reviewed. Based on these, research characteristics of the two methods are analyzed.

Keywords:
Biosensor / Microfluidics / Single cell analysis / Tumor cells
DOI 10.1002/elps.201800413

1 Introduction

Cancer is the second leading cause of death globally. According to the cancer country profile published by World Health Organization (WHO) in 2014, there are 2,656,000 cancer deaths in the United States of America, 9,846,000 in China, and 9816,000 in India. However, nearly 1 in 6 deaths is due to cancer in the world. Cancer can start almost anywhere in the human body, and cells become more and more abnormal and divide without stopping when it develops [1]. These extra cells may form growths called tumors. Cancerous tumors are malignant, and some of which called circulating tumor cells (CTCs) can break off and be transported in circulatory blood to distant organs forming new tumors [2]. Thus, tumor metastasis is the main cause of treatment failure, and more than 90% of cancer patients die from tumor metastasis [3–5]. Therefore, detection of CTCs is of great significance for clinical diagnosis and has attracted wide interests due to its potential advantages such as repeatable and noninvasive [6,7].

Realizing accurate CTCs detection is difficult in the early stage of cancer due to the low number of CTCs in peripheral blood. The traditional methods of CTCs detection consist of flow cytometry and isolation by size of epithelial tumor cell [8,9]. For the former, a commercial system named CellSearch developed by Johnson & Johnson is the most representative equipment of CTCs detection. It was certified by FDA in America in 2007, and entered Chinese market in 2013. However, flow cytometry is a mature technology and of high accuracy, but is limited due to high operation costs and bulky instruments [10]. On the contrary, the latter method is simple to use and inexpensive, but with higher probability of missed detection for nontumor cells that have the similar density with that of tumors.

In recent years, microfluidic technologies of high integration and good biocompatibility offer outstanding advantages for tumor cell detection. Microfluidic technology means manipulating and controlling fluidic in submicron degree in microchannels that have the functions of reagent mixing, separating, analyzing, and detecting. It is also known as "lab-on-chip." It was only applied in chemistry domain on the initial stage due to the complicated processing technic of device fabrication [11–13]. However, later in 1998 the procedure was simplified by Whitesides et al. who fabricated microchannels in an ordinary laboratory with the help of a commercial printer. This experiment took advantage of soft lithography and its achievement of easy fabrication of micro devices promoted the development of microfluidic technologies in many research fields. Together with the material of PDMS that has good biocompatibility, microfluidic technology has gradually been applied to biomedical field [14, 15]. Such as RNA and DNA amplification [16,17], single-cell analysis [18,19], "artificial lung" that represents research of organ on a chip [20] [21], and even study on the conceptualization of human on the

Correspondence: Dr. Feifei Tan, College of Communication Engineering, Chengdu University of Information Technology, No. 24 Block 1, Xuefu Road, Chengdu, Sichuan 610225, P. R. China
E-mail: tffcool2007@126.com

Abbreviations: **CTC**, circulating tumor cell; **DEP**, dielectrophoresis; **DLD**, deterministic lateral displacement; **EMA**, electroactive microwell array; **EP**, electrophoresis; **EpCAM**, epithelial cell adhesion molecule; **FL**, fluorescent light; **RBC**, red blood cell

Color online: See article online to view Figs. 5–16 in color.

chip [22]. Thus, microfluidic technologies for tumor cell detection that belongs to single-cell analysis category have been developing these years.

The purpose of introducing microfluidic techniques to tumor cell detection is to achieve point-of-care diagnosis in the early stage of cancer with precision and low-cost. Since the quantity density of CTCs in peripheral blood is proportionally correlated to metastases, most of the related researches concentrated on CTCs trapping and enumeration [23–25]. For example, Xia et al. designed a micro-magnetic activated cell sorting chip with a trapping efficiency of 72.8% aiming at human colon cancer cells [9]. In reference [26], a new poststructure array consisting of a multiple concave surface design has been fabricated and tested. Its capture rate of repeated measurements is higher than that of a traditional circular structure in [27] that is about 65%. Jinhong Guo et al. proposed a microfluidic impedance cytometer based on a solid-state micropore for detection and enumeration of cancer cells from red blood cells [28]. Different concentrations of Hela cells were tested by both the microfluidic sensor and a commercial cytometer (FC500, Bechman Coulter, CA, USA). Excellent consistency of the two testing methods was demonstrated.

However, the applications of microfluidic technologies in CTCs detection are based on different physical principles, such as the use of magnetic field and micropost mentioned above. Extra force fields can cause different cell deformations and flow paths due to the different characteristics between tumor cells and other cells in blood. Combine with well-designed micro structures, the target tumor cells can be isolated. If there is no extra force field, cells can also be captured by micro devices with cellular level fabric based on the different sizes between target cells and others. This paper will give a review about microfluidic technologies for tumor cell detection based on different physical principles.

Based on whether extra force field is applied, the methods of microfluidic technology for CTCs detection can be categorized into two types, active and passive methods. Active methods refer to the introduction of a kind of extra force field in the detection except the inertial force of the cells induced by flowing in a microchannel. These extra force fields can be generated by optical beams [29–31], electrodes [32, 33], magnetic concentrators [34, 35], and ultrasound [36–39]. Conversely, if there is no extra force field, it is called the passive method. Some common active and passive methods are listed in Table 1, and will be discussed in the later sections.

Table 1. The classification of microfluidic principles for tumor cell detection

Active	Passive
Optical energy	Mechanical filtering
Electric field	Inertial microfluidic
Magnetic field	
Acoustophoresis	

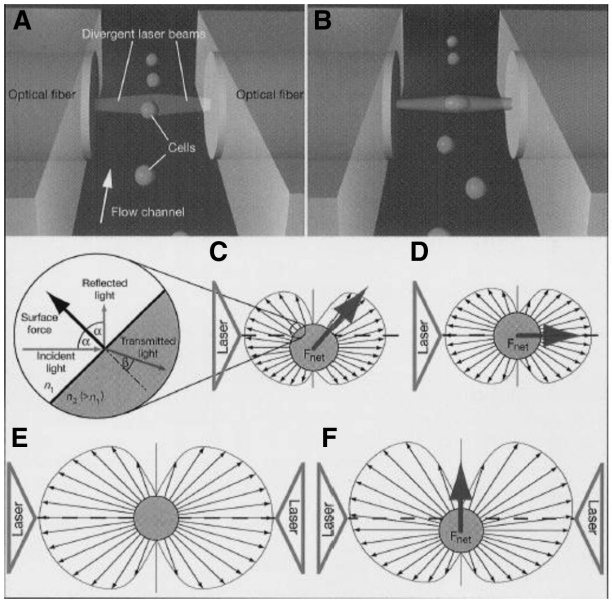

Figure 1. Shows the optically induced surface forces lead to trapping and stretching of cells [30].

2 Active methods for tumor cell detection

2.1 Optical energy

Optical energy can be applied for tumor cell detection due to its influence to cells. Optical tweezers refer to a single beam gradient force optical trap that can be used for trapping and stretching of biological samples including living cells [40, 41]. Cells flowing through a microfluidic channel can be serially trapped and deformed with two counter propagating divergent laser beams [30]. The momenta of the various light rays and the resulting force at the surface of a cell is presented in Fig. 1. The small arrows show the distribution of surface forces induced by one laser beam with Gaussian intensity profile. C and D show the conditions of one laser beam (the large triangle) incident from the left for a cell that is slightly below the laser axis (C) and on axis (D), respectively. All these forces over the entire surface result in the net force F_{net} shown as the large arrow. When placing two identical but counter propagating laser around a cell on the axis as shown in E, the cell is trapped and stretched. The setup of this microfluidic optical stretcher was essentially the same as described in reference [42], as shown in Fig. 2. The fiber laser was spliced to a coupler to ensure equal power in the two fibers. The laser power was 100 mW per fiber for trapping the cells. The optical deformability of human breast epithelial cells and their cancerous counterparts have been measured. The cell lines are shown in Table 2. Figure 3 shows the typical examples of the stretching of breast epithelial cells. A and B are nonmalignant MCF-10 cells, C and D are cancerous MCF-7 cells, E and F are metastatic modMCF-7 cells. The images in the left column are taken at an incident light power of 100 mW in each beam while these in the right column are

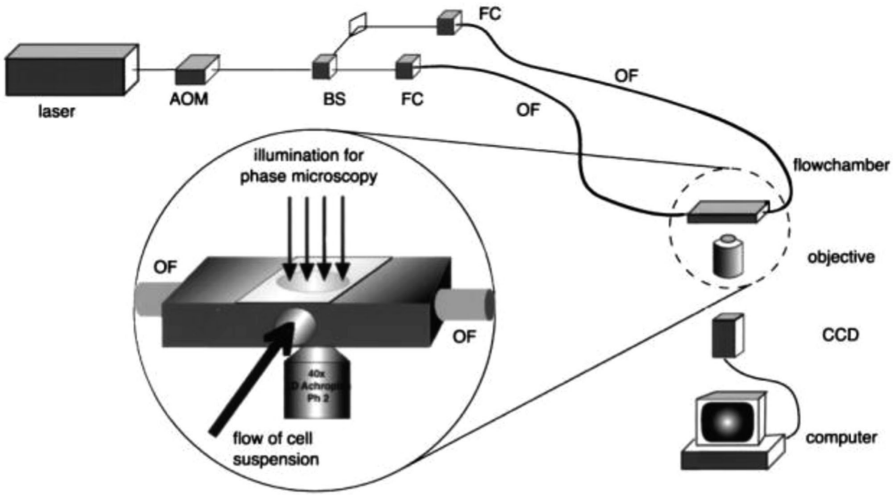

Figure 2. Shows the setup of the optical fibers in [42].

taken at 600 mW. The cells in the right column are trapped. The optical deformability of cell groups MCF-10, MCF-7, and modMCF-7 in Table 2 are shown in Fig. 4A. The optical deformability of cell groups MDA-MD-231 and mod MDA-MD-231 in Table 2 are shown in Fig. 4B. It is obviously that the cells deform when the incident light power is higher (the right column). And the higher the transferability is, the more deformation happens. The five populations of cell are clearly distinguishable in the histograms of the measured optical deformability. The rate of trapping cells from a flowing cell suspension and measure their deformability is 1 per min. This work demonstrated that optical deformability is sensitive enough to monitor the subtle changes during the progression of human breast epithelial cells from normal to cancerous and even metastatic state. It promotes research in using optical deformability as an inherent cell marker for cell investigation and diagnosis of disease.

Recently, Guo et al. proposed a compact optofluidic cytometer for tumor cell detection and enumeration [43]. This device includes the microfluidic focusing and optical detection components on a glass substrate made with poly. The schematic of the device is shown in Fig. 5. It consists of a flow component and a detection component. Samples are introduced from inlet A. Inlets B and C are used to convey the sheath flow to keep the sample focused at the center of the microchannel. In the detection region, the excitation fiber is used to guide the excitation light, and the air lens help focus the laser light on the sample flow stream. There are three detection fibers, forward scattering, side scattering, fluorescent light (FL), are used to measure three optical parameters respectively. In order to evaluate the accuracy of the device for enumeration of CTCs, specific concentrations of Hela cells are tested by both the optofluidic chip and a commercial flow cytometer, the total number of the cell events recorded by the optofluidic chip is in good agreement to the commercial flow cytometer. The proposed device in this work has very low cost and highly portability compared to the conventional flow cytometers.

2.2 Electric field

There are two main methods in the applications of electric field for CTCs detection, Coulter principle, and dielectrophoresis (DEP). Coulter principle is a powerful tool for the detection and enumeration of biological particles or cells in fluidic electrolyte solution [44], and has found typical utilization in commercial equipment called Coulter counter. The principle can be expounded as follows: there are two chambers with an electrode in each. The chambers are separated by a shelf that has a micro hole in the center. When the sample is injecting into the chamber, it flows into the other chamber under pressure and become a liquid bridge between the two electrodes. The pressure can be produced by several means that depend on the specific design. For example, in the device designed in reference [45] cells experience three kinds of forces, electrophoresis force due to the applied electrical field, dielectrophoresis force due to the nonuniform electrical field near the aperture in the structure, and hydrodynamic force due to the carrying flow field. However, when cells are right in the hole, significant electrical current change happens because these cells displace the conducting electrolyte solution. By analyzing the change of electrical pulse amplitude and pulse bandwidth, the information of size and numbers of the cells can be acquired.

Another method is dielectrophoresis. This method is based on electrophoresis. In an uniform electric field which, for example, generated by two parallel metal sheets, charged particles will move toward the metal sheet with opposite polarity. This phenomenon is called electrophoresis (EP). To utilize EP, electrostatic field must be applied and the particles in medium should be charged. Under the same condition, particles migrate at different rate that usually is related with the amount of charge they carry, the electric field intensity and molecular size and shape. Therefore, EP is more suitable to be used to analysis molecules and ions, such as enzymes [46], proteins [47], DNA [48], peptides [49], plasmas [50], and several ions [51, 52].

For biological cell that usually consists of organic molecules and inorganic ions, an electrostatic field will not make it move due to its electrical neutrality. In this case, we can put the neutral particle in an uneven electric field to make it polarized and move under a force caused by the inhomogeneity of the electric field. This phenomenon is essentially produced due to the dielectric property of the particle, so it is called DEP. The DEP force that the neutral particle is experienced can be expressed as Eq. (1) [53]. ε_m is the dielectric constant of solution, r is radius of the particle. K(ω) is Clausium-Mossotii that is determined by the dielectric constants of both solution and particle, their mathematical relationships can be expressed in Eq. (2) [53]. E_{rms} is the root mean square of applied electric field strength. According to Eq. (1), particles with different sizes and dielectric constants will experience different DEP forces that lead to diverse motion speeds and trails. Together with specific devices, particles isolation can be realized. According to Eq. (2), if the dielectric constant of the particle ε_p is larger than that of the solution, then Re [K(ω)]>0, the particle will move toward the highest point of applied uneven electric field. Conversely, it will move toward the lowest point.

$$F_{DEP} = 2\pi\varepsilon_m r^3 \mathrm{Re}[K(\omega)] \nabla E_{rms}^2 \quad (1)$$

$$\mathrm{Re}[K(\omega)] = \frac{\varepsilon_p - \varepsilon}{\varepsilon_p + 2\varepsilon_m} \quad (2)$$

Guo et al. created a microfluidic cytometry for tumor cell detection and enumeration [45]. Its work principle is similar with Coulter counter but not huge or expensive. The fabricated device is shown in Fig. 6. (a) is the exterior of the microfluidic chip and tubing that are positioned on a microscope stage that was housed in a Faraday cage. (b) is the microscopic image of the central chip structure. (c) is the experimental setup for observation and electrical measurement by a patch clamp. (d) is the schematic circuit of the

Table 2. The cell lines and the related characteristics

Method	Cell lines	Cells characteristics	Captured/recovery efficiency	Throughput/flow rate	Reference
Optical tweezer	MCF-10	Noncancerous but otherwise normal;	—	1 per min	[30]
	MCF-7	Cancerous			
	modMCF-7	Dramatic increase in the metastatic potential.			
	MDA-MD-231	Highly metastatic.			
	ModMDA-MD-231	Cancerous			
Electric field	Tumor cells	Cancerous	38.2%±2%	5 μL/min	[54]
	MDA231	Metastatic	> 50%; Viability 80%	5 μL/min	[58]
	SKOV3	Metastatic	75.4%±3.1%	2×10^5 cells/min	[61]
	MDA-MB-231	Metastatic	71.2%±1.6%; Viability >97.1%	2×10^5 cells/min	[61]
	HTC116	Cancerous	57%	0.1 μL/min	[60]
	Hela cells	Cancerous	76%	NG	[62]
Electric field and hydrodynamic	MCF-7	Cancerous	93.31%	126 μL/min	[64]
Magnetic field	Vcap	Cancerous	>80%	33 μL/min	[75]
Acoustophoresis and magnetic field	DU145	Cancerous	96±0.8%	20 μL/min	[77]
			65±13%	100 μL/min	
Microsieve	MCF-7	Less invasive	83±3%; Viability 74±2%	—	[91]
	MDA-MB-231	High invasive	78±4%; Viability 71±9%	—	
	MCF-7	Less invasive	71.1±5.6%; Viability 98.2±1.3%	5 mL/h	[92]
	MDA-MB-231	High invasive	70.3±10.9%; Viability 93.6±4.5%	5 mL/h	
Inertial microfluidic	MCF-7	Cancerous	85%	1.7 mL/min	[101]
	T24	Cancerous	80%	1.7 mL/min	
	MDA-MB-231	Metastatic	87%; Viability >90%	1.7 mL/min	

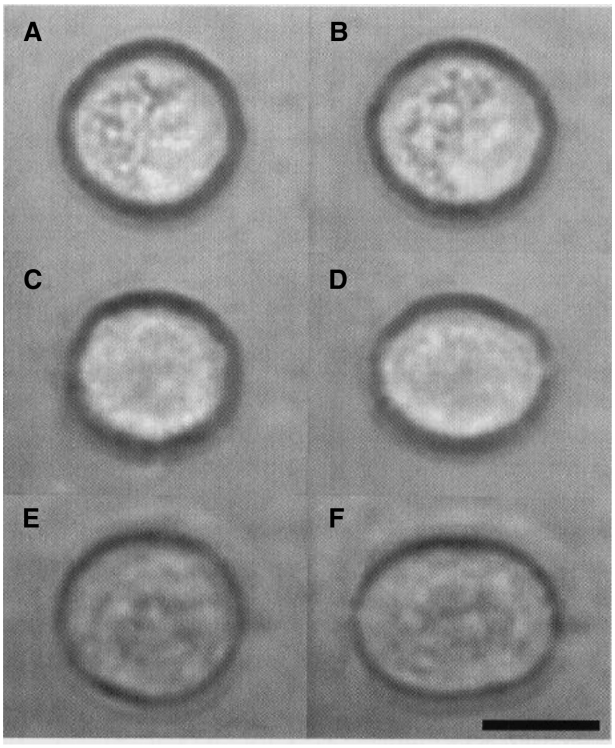

Figure 3. Shows the typical examples of the stretching of breast epithelial cells in [30]. The scale bar at the lower right corner is 10 μm.

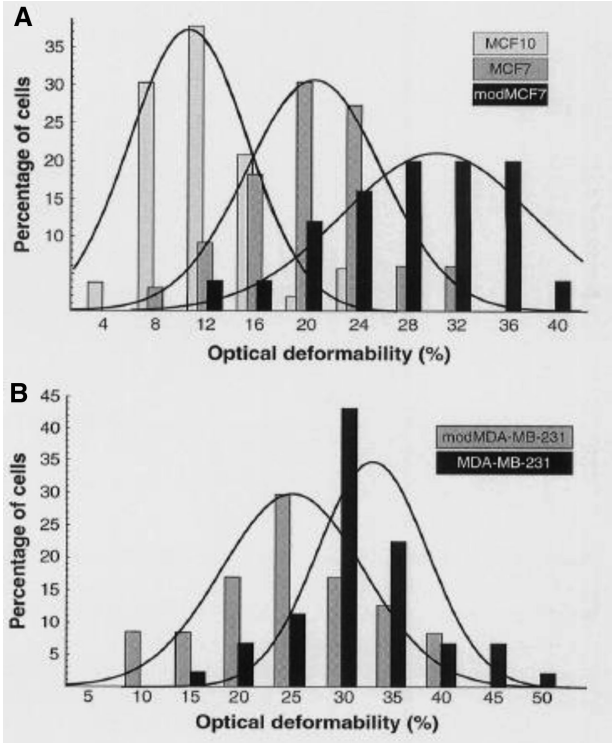

Figure 4. Is the optical deformability of the three cell lines. The values were measured at $t = 60$ s [30].

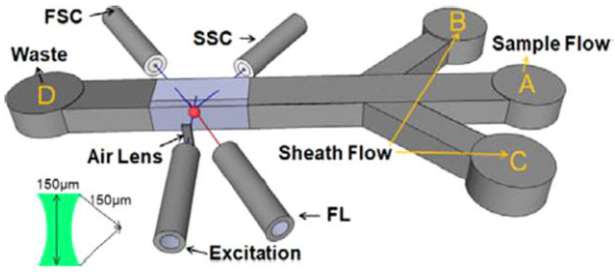

Figure 5. The schematic view of the optofluidic cytometer in reference [43].

chip. This chip has four channels named A, B, C, and D. A and B are the inlet and outlet for the sample, respectively. C and D are the liquid channels that act as the conducting electrodes. The length and width of the sensing aperture in the shelf are 150 and 25 μm, respectively. When the particle approaches very closely to the sensing aperture, the channel resistance starts to change significantly that leads to changes in electrical pulse. This device has been used to test polystyrene particles with different sizes, and the results were compared with the simulated ones so as to demonstrate that it can count the number of cells by testing the pulse width. In this work, the testing pulse amplitude and width are two key elements of distinction between target cells and other particles. It can provide critical insight and guidance for developing the novel micro-Coulter counter. But the flow rate is 1.5 μL/min that is relatively low.

Based on this, the same research group exploits support vector machine algorithm in order to improve the accuracy in CTCs detection [54]. The microfluidic sensor comprises a micropore on an 8-inch silicon wafer and a plastic package. As shown in Fig. 7. The dimension of the whole device is 5 × 5 $cm.^2$ The fabrication of the proposed device is simple and can be accomplished in a laboratory. The theory is the same with their prefer work, the current change due to the blockage of the particle is linearly proportional to the particle volume. A syringe pump was used to perfuse the sample flow through the main channel at a flow rate of 5 μL/min. It is important of promoting the flow rate to avoid blood coagulation in CTCs detection at the stage of clinical applications. Three samples of Hela cells with different concentrations have been tested using the proposed microfluidic sensor and the commercial cytometer, respectively. The test results are in good agreements. In addition, the translocation time of a single cell is another important parameter in analyzing the biological cells using Coulter principle. This is because the cell will become longer in shape in the direction of the flow when it goes through a narrow aperture due to the flow shear stress. Obviously this deformation will increase its translocation time. Since CTCs are easier to be deformed [55, 56], translocation time can be used to distinguish CTCs from other cells in blood. Two samples of RBCs (red blood cells) and CTCs were both tested by the device, and totally about 523 cell events were measured and analyzed. The conclusions indicate that

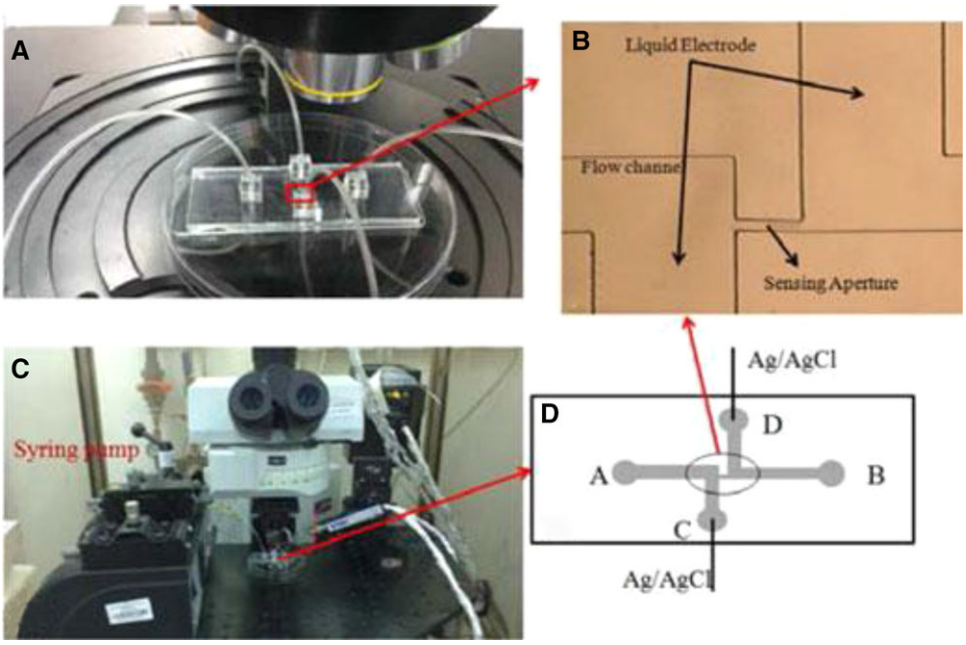

Figure 6. The schematic and microfluidic chip designed in [45].

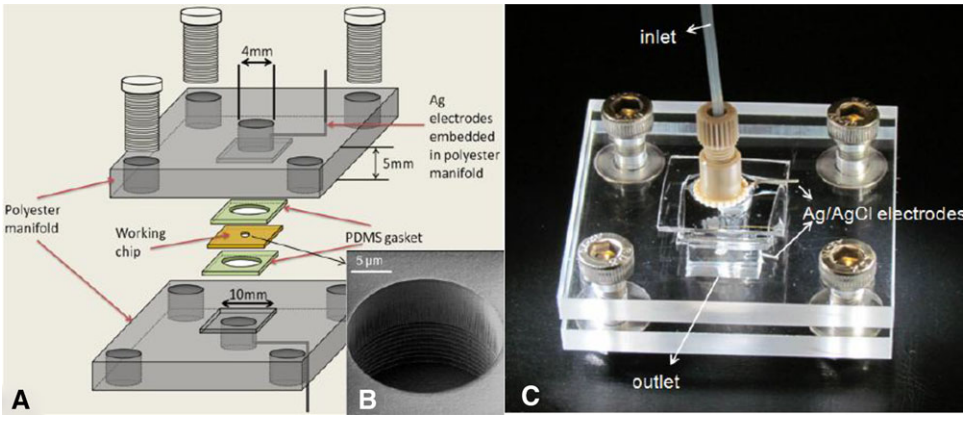

Figure 7. The schematic view of the impedance cytometer in reference [54].

translocation time of tumor cells is much longer than RBCs due to their larger sizes. In addition, a sample mixed with RBCs and tumor cells were tested. Total of 231 tumor cells were detected by the proposed device and a capturing efficiency of 38.2%±2% was obtained with three independent test runnings. As a comparison, sample with the same parameters has been tested by the commercial flow cytometry and obtained a corresponding percentage of 36.4% ± 0.5%. However, the results of the two equipments are accordant with each other, but the tested boundary between RBCs and CTCs in the mixed sample is less clear when compared to that in the individual training test. However, this research goes further by integrating a microfluidic differential coulter counter to a portable system [57]. In this system, the microfluidic differential coulter counter is built on the metal-oxide-semiconductor imaging sensor with white light illumination. For different cell types, the system will detect differential resistive pulses. Each pulse activates an on-demand imaging of single cells. Cell mixture including RBCs and HepG2 has been used to validate the system and 7 RBCs and 4 HepG2 (a hepatoma tumor cell line) cells have been counted and differentiated.

The above methods can potentially provide solutions for relatively reliable and low cost platform for tumor cell detection from circulating blood cells, but the highest throughput is only 5 μL/min that is relatively low.

Becker et al. found a way to separate human breast cancer cells from blood that is in the early stages of dielectricl-based cell isolation [58]. This work demonstrated that the dielectric properties of the metastatic human breast cancer cell line MDA-MB-231 were significantly different from those of erythrocytes and T lymphocytes. These differences were exploited to capture the cancer cells from diluted blood under electrorotation forces. The microfluidic device contains a 17.6 mm × 55 mm array of interleaved gold electrodes on a glass substrate. All tumor cells remained on the electrode tips with voltage applied, while the other cells in blood were retained in the chamber. The purity of the tumor cells is more than 95%.

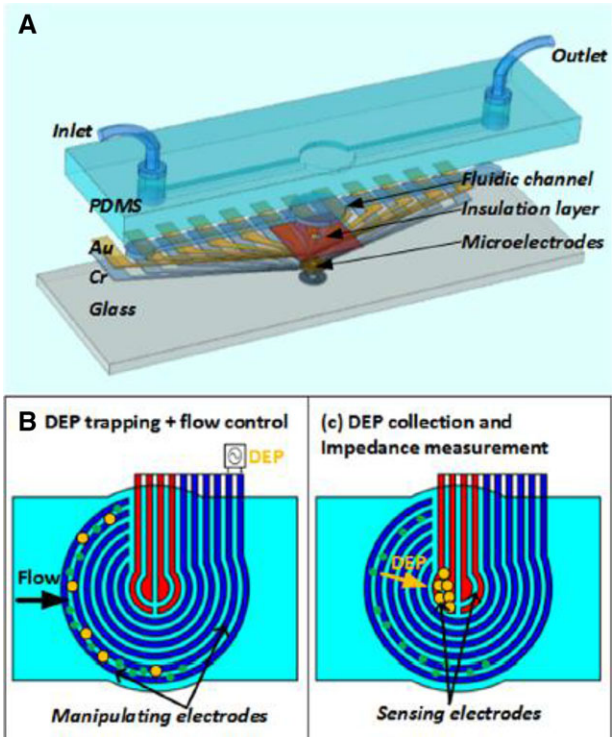

Figure 8. The structure of the proposed microfluidic device in [59].

Ngoc-Viet Nguyen et al. have gone further [59]. They proposed a microfluidic device with double pairs of symmetrical sensing microelectrodes that combines DEP manipulation and impedance detection together. There are two parts in the circular electrodes as shown in Fig. 8. The outside blue region is for DEP manipulation. CTCs are collected and consequently focused from here into the central red region that is for detection. In this work, an enrichment rate of over 90% for A549 human lung CTCs has been achieved. Besides, the device has relatively high sensitivity due to the fact that it can detect this cell line with very low cell number (approximately 3 cells).

Like many early DEP-based methods [60–63], one of the deficiencies in these works is that the electrodes are directly exposed to the medium. This will lead to bubble formation due to electrode fouling and electrolysis, and sample contamination [65, 66]. Therefore, some researchers concentrated on contactless dielectrophoresis method. However, to obtain a sufficient DEP force from contactless electrodes, a great high voltage will be applied that can up to several hundred volts [67] [68]. High strength of voltage could result in rupture of the cell membrane and cell lysis [69, 70], and device instability.

Gupta's group developed a device called ApoStream™ that has been commercially available [61]. The setup of the device is shown in Fig. 9. It also uses DEP technology in a

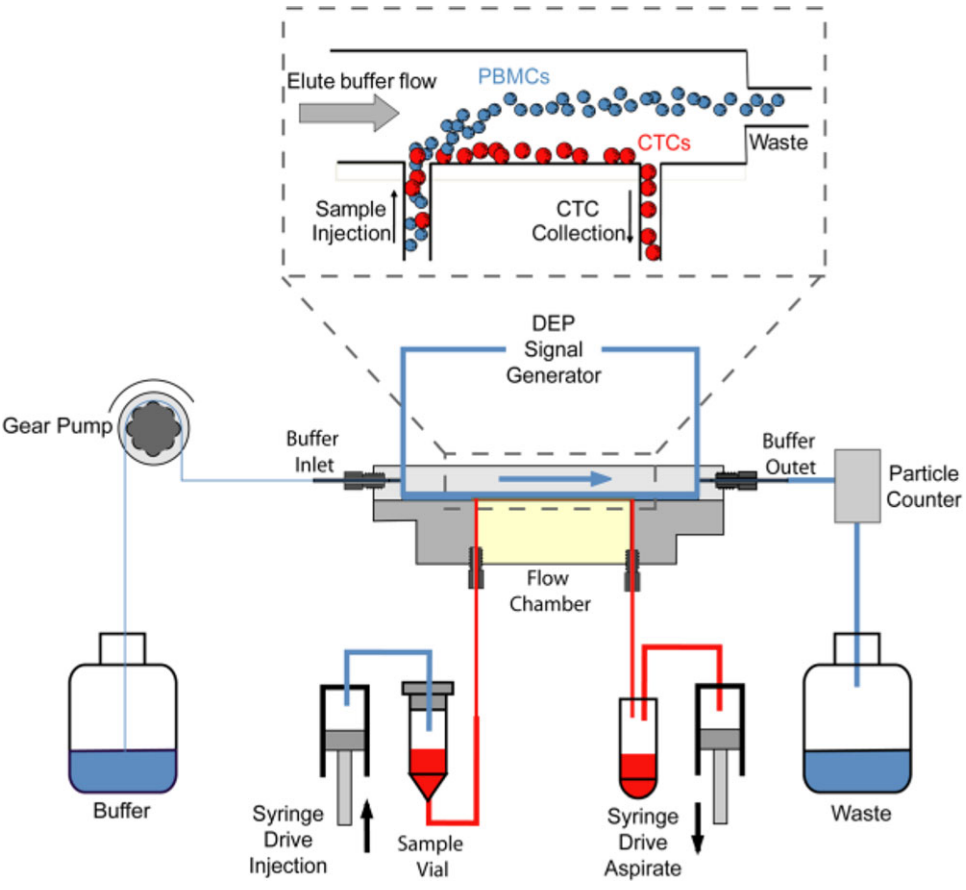

Figure 9. The complete setup of the ApoStream™ device in reference [61]. The sample is injected at a low flow rate into the bottom of the flow chamber to ensure cells stay within the effective DEP field. The DEP forces pull cancer cells toward the chamber floor and repel other cells as they traverse the electrode.

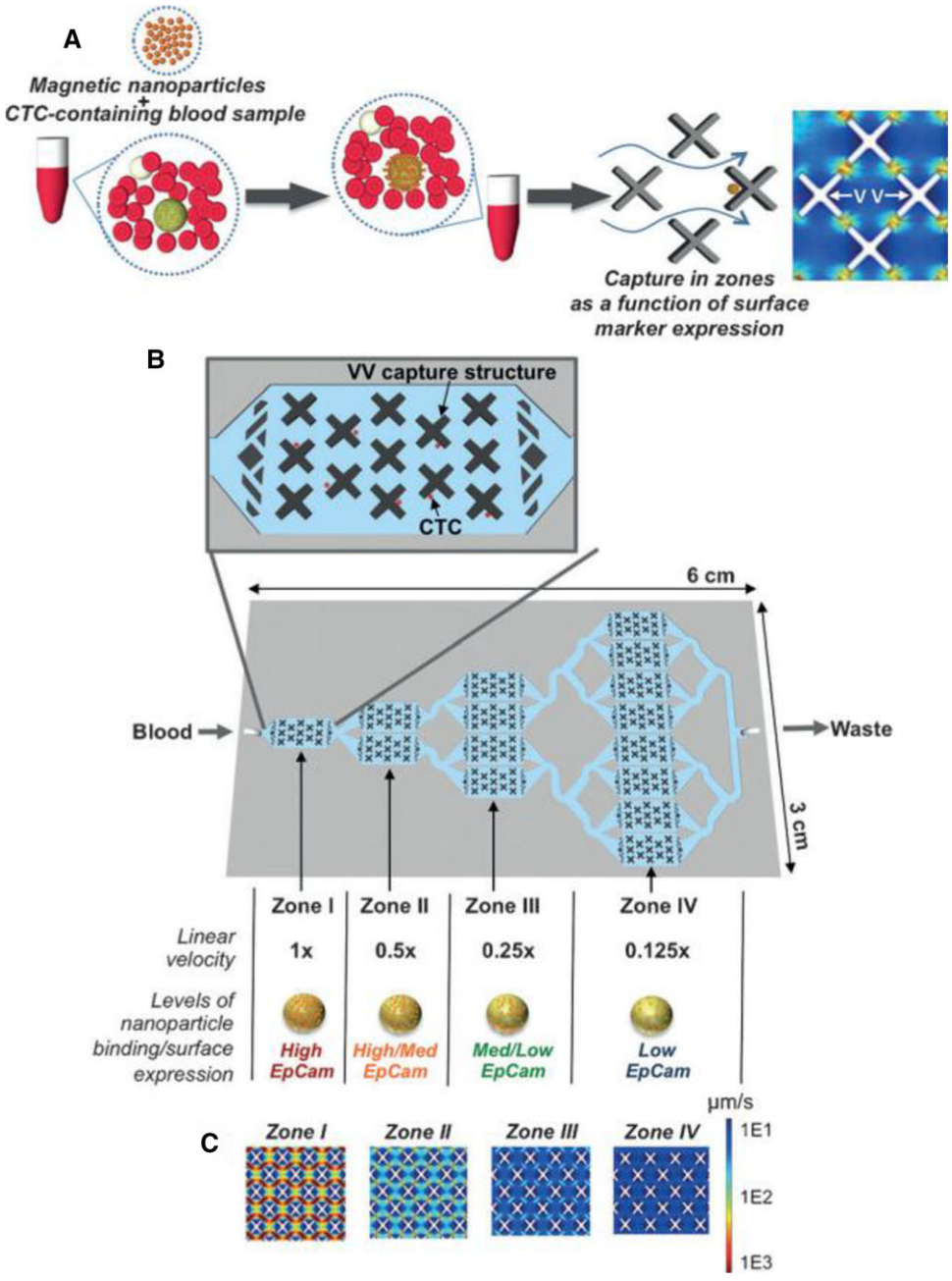

Figure 10. Design of a device for surface-expression-guided binning of heterogeneous circulating tumor cells. It is cited from [75].

microfluidic chamber to isolate and enrich CTCs from blood. The floor of the flow chamber consists of a flexible polyimide film sheet with electroplated copper and gold electrodes, the ceiling of the flow chamber is formed by an acrylic sheet, and the two side walls of the chamber are made of gasket. The DEP forces pull cancer cells toward the chamber floor and repel other cells as they reverse the electrode. The cancer cells are injected at a low flow rate to stay with the effective DEP field. This device has advantages of antibody independent, high throughput, and efficient isolation, and enrichment of CTCs from blood, according to Table 2. The research in reference [61] indicates that the device has the potential to isolate and recover viable cancer cells from all cancer types that contribute a lot in the field of CTCs detection.

2.3 Magnetic field

Molecules and cells bound to magnetic particles can be isolated by taking advantages of the magnetic forces [71–74]. Reza M. Mohamadi's group developed an X-shaped microfluidic device to trap and distinct CTCs relying on the tagging of cells with magnetic nanoparticles [75]. Specifically, CTCs are tagged with magnetic nanoparticles functionalized with

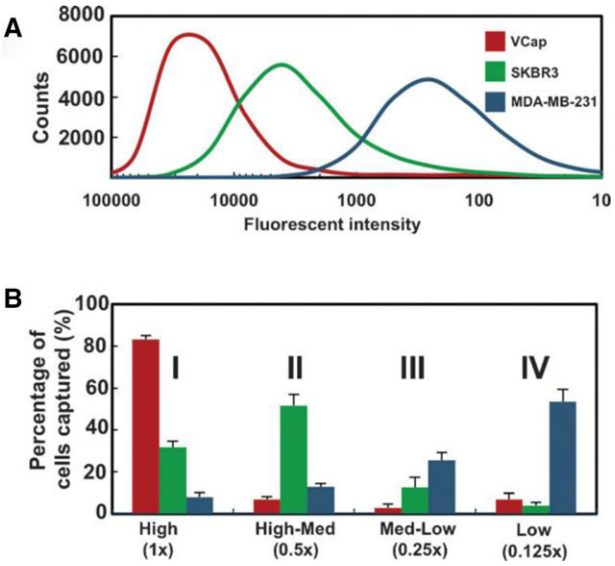

Figure 11. Results of the three tumor cell groups. They are cited from reference [75].

an antibody against the surface marker, epithelial cell adhesion molecule (EpCAM). Some studied have shown that the metastatic potential of CTCs has something to do with the degree of EpCAM loss. Epithelial markers of CTCs may be gradually lost when they are undergoing the epithelial to mesenchymal transition [76]. Therefore, the levels of epithelial markers of CTCs can be used as a predictor of cancer recurrence. The schematic of the device is shown in Fig. 10. The low magnetic susceptibility of nanoparticles leads to a low magnetic force is easily overcome by the drag force that is created by the local velocity valleys in Fig. 10. That is to say, CTCs with different EpCAM expression levels can be distinguished by capturing them in different zones. The microfluidic device with four sorting zones successfully captured three cell lines of Vcap, SKBRS, and MDA-MB-231 in the multizone device as shown in Fig. 11. It developed a new way to analyze CTCs and discrete CTCs subpopulations by tagging cells with EpCAM-targeted nanoparticles.

2.4 Acoustophoresis

Acoustophoresis is another method that can be used for tumor cell detection. Like the methods mentioned above, it is also simple, fast, biocompatible, contact-free, label-free, and easy to integrate with other microfluidic technologies. The difference is that this method exploits the primary acoustic radiation force on particles, which is caused by ultrasound standing waves and strongly dependent on the particle sizes [78–80]. Then, cells will be focused into the pressure node or anti-node by the force.

Soo Hyeon Kim's group proposed a microfluidic system by integrating an acoustofluidic chip to an original electroactive microwell array (EMA) [81]. The integrated device is shown in Fig. 12. Acoustophoresis utilizes ultrasound standing waves to focus cells into the pressure node or anti-node so as to preconcentrate the sample. Subsequently the EMA utilizes dielectrophoresis (DEP) attracts the cells to the bottom of the microwells. The combination of the two chips was demonstrated to be able to improve the sample throughput capability. It was 10 times that of the DEP-trap alone.

However, this work didn't allow for direct processing of clinically relevant samples since it doesn't have a separation function. The same research group then developed a novel integrated device aiming at minimizing rare cell loss in the postseparation sample processing steps, by integrating the separation with the trapping and on-chip analysis [81]. The updated system benefited from the integration of two original microfluidic devices as well. Different from the prior design, the acoustofluidic device was used to prealign, separate, and concentrate the target cells.

3 Passive methods for CTCs detection

In contrast with active methods, passive microfluidic devices rely on fluid forces and channel structures to achieve cell isolation rather than extra forces. The theoretical reference is to exploit the size and shape differences between tumor cells and other cells in blood. These microfluidic chips are simpler and easier to obtain high throughput. In detail, passive methods consist of mechanical filtering, hydrodynamics, and inertial microfluidics [82]. Most of the researches concentrate in mechanical filtering and inertial microfluidics.

3.1 Mechanical filtering for tumor cell detection

These isolation methods take advantage of the fact that tumor cells are usually larger than normal blood cells. It consists of microsieve, pillar, weir, or cross-flow in microfluidic device to change flow field distribution in microchannels, then the flow track of cells with different sizes and deformabilities will be separated.

The early research on microfluidic particle-separation based on micropost structure is carried out by Lotien Richard Huang's group [83]. The separation process uses laminar flow [84, 85] through a periodic array of micropost, and it is called deterministic lateral displacement (DLD). There are two situations. One is called "zigzag mode."

As shown in Fig. 13B, there are three lanes. Particles that are smaller than the lane width starting from any of the three lanes in will go back to the original lane assignment after three rows. Therefore, the migration is in the average flow direction. The other is called "displacement mode" that is in contrast with the smaller particles. This transport pattern is for particles with the radius larger than the width of lane 1. The black dot in Fig. 13 represents a larger-particle, it is physically displaced as it enters the next gap, and the black dotted lines mark the lanes. DLD method has advantages of

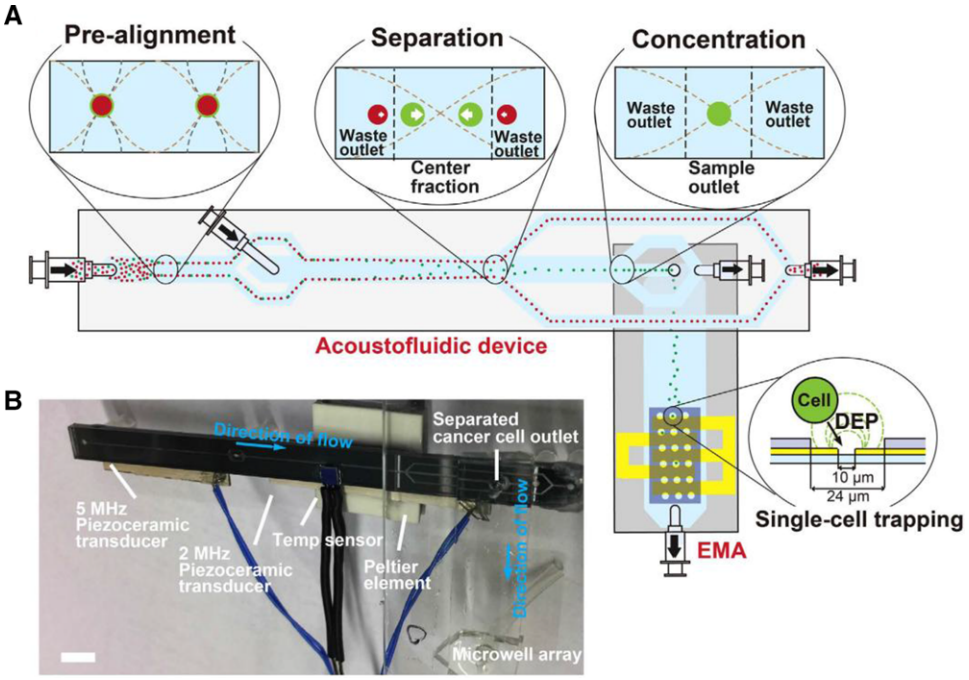

Figure 12. The integrated device in reference [81]. (A) There are three operation zones in the acoustophoresis chip. White arrows in the separation cross-section indicate the lateral acoustophoretic force. (B) Integrated device showing the acoustic chip directly bonded to the chip. This work is licensed under a Creative Commons Atrribution 4.0 International License. http://creativecommons.org/licenses/by/4.0/

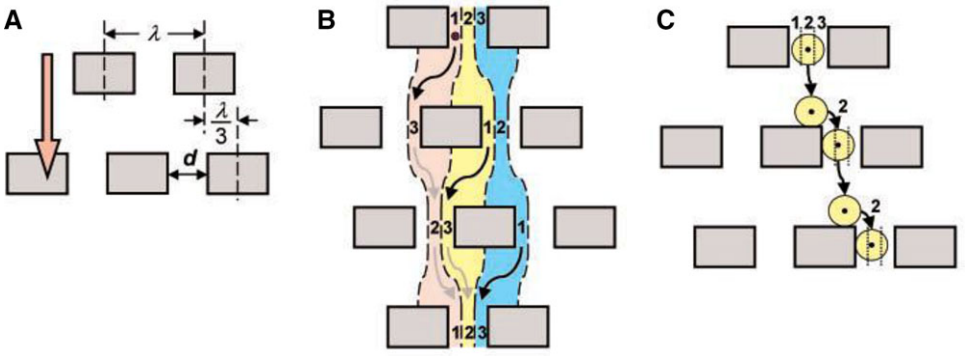

Figure 13. The separation process in reference [83].

high resolution, but leads to complexity in device designing and low throughput compared with active isolation methods.

The simplest structure of mechanical filters is microsieve. It contains many pores on a 2-dimensional layer [86–90]. Microsieve devices offer high throughput (> 10 mL/h) [82] and simple work principle but has a high probability of damage to the captured CTCs due to the high flow rate and filtration pressure.

Addressing this shortcoming, Ming-Da Zhou's group proposed a separable bilayer microfilter for viable size-based CTC capture [91]. Unlike other single-layer CTC microfilters mentioned above, this work contains two layers with precise gap between them. As shown in Fig. 14A, the two layers and architecture of pore alignment make tumor cells captured along the edges of the large top layer. This kind of design may lead to big reduction in mechanical stress on CTCs so as to reduce damage to the captured cells. However, this work is to provide a transformative approach to detect CTCs.

Jiyoon Bu et al. proposed a fabric filter to further minimize the cell damage [92]. The fabric filter is composed of 20 denier polyester monofilament yarns. In order to separate cancer cells, the holes formed in between the neighboring warps and wefts are used as micro-sized slots. Two human breast cancer cell lines, MCF-7 and MDA-MB-231 have been tested by this device. To validate the reduction of mechanical stress applied on cells, they numerically analyzed and compared the stress applied on the microsized rubber beads that were used to replace cells since it is hard to obtain exact mechanical characteristics of cells such as viscosity or stiffness. It was shown that the stress applied to the cells in the fabric filter was 21.6% reduced. And the viabilities for the two cell lines are much higher than that in [91] and some other relative works [88, 89].

3.2 Inertial microfluidic for tumor cell detection

Inertial microfluidic technique exploits particles' inertial and secondary flow under inertial force [93]. Particles or cells flowing in a microchannel are subjected to two dominant forces:

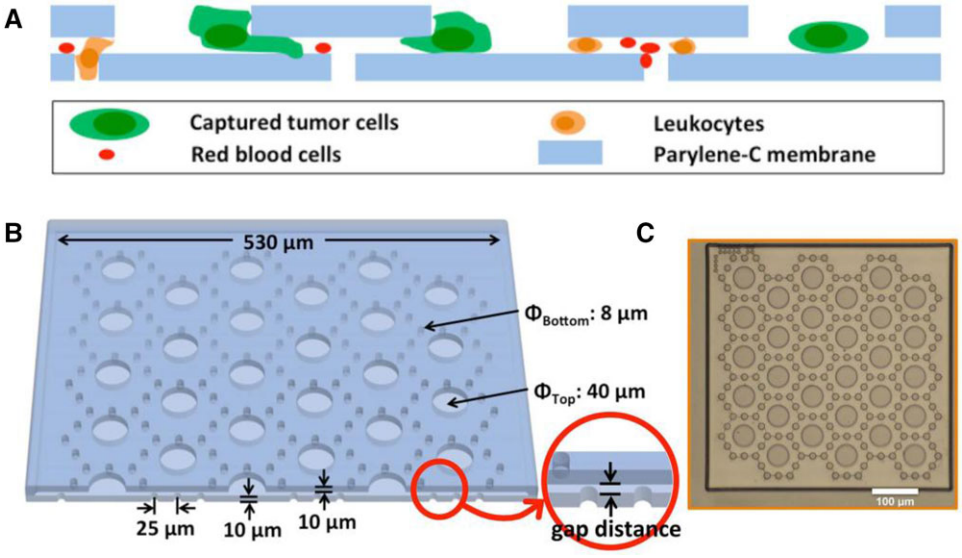

Figure 14. Device design in reference [91]. This work is licensed under a Creative Commons Attribution NonCommercial-ShareAlike 4.0 International License. http://creativecommons.org/licenses/by-nc-sa/4.0/

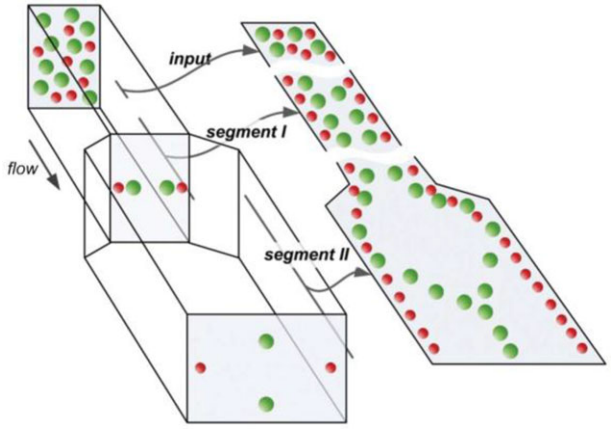

Figure 15. Schematic diagram of the design concept in reference [98].

the viscous drag (F_D) and the inertial lift force (F_L). F_D entrains particles along streamlines, and F_L leads to migration across the streamlines. In 1963, Segre and Silberberg first observed particle migration in a cylindrical tube with 1 cm in diameter [94, 95]. At first, rigid particles flow in a cylindrical tube at random positions. After flowing with the fluid for some distance, they will gradually converge into rings on the cross section. This phenomenon has been confirmed by many researchers and attracting considerable interests in recent years [96, 97].

Jian Zhou's group developed a modulation of aspect ratio for complete separation system based on inertial microfluidics [98]. It contains two segments build on the model of two-stage migration in rectangular microchannels. The upstream segment I in Fig. 15 consists of a high aspect ratio where randomly dispersed particles order in two equilibrium positions at the centers of the channel sidewalls. Then the downstream segment II transition to a low aspect ratio microchannel equilibrium positions shift to centers of the top and bottom walls. Since the larger particles complete their migration much faster than the smaller particles, the larger particles in segment II equilibrate near centers of the top and bottom wall while the slowly migrating smaller particles remain near channel sidewalls. This work demonstrates an isolation of rare cells in blood spiked with human prostate epithelial tumor cells.

In the system above, it uses straight channels with rectangular cross-section that has the advantage of simple structure, thus particles can gather in the center line along the width direction. This kind of structure makes the design of distribution system at the outlet simpler. On the other hand, the number of equilibrium positions in a rectangular tube is fewer than that in a circular or square tube, which also facilitate efficient distribution design.

Another structure is curved channel in where particles experienced Dean force. The Dean rotational force is induced by the secondary flow when fluids flow through a curved channel and can achieve more accurate manipulation. This original dimensionless number that describes the magnitude of this flow was first established by W. R. Dean [99].

Papautsky's group proposed a microfluidic device based on the principle of Dean-coupled inertial migration in spiral microchannels [100]. The equilibrium positions of the particles are dependent on the ratio of the inertial lift to Dean drag forces. This device features a high throughput of 1,000,000 cells/min, and can separate neuroblastoma and glioma cells with 80% efficiency.

Majid Ebrahimi Warkiani' group later proposed a device [101] that is similar in shape of reference [100]. It has single spiral microchannel with one inlet and two outlets, as shown in Fig. 16. CTCs focused near the inner wall due to the combination of the inertial lift force and the Dean drag force

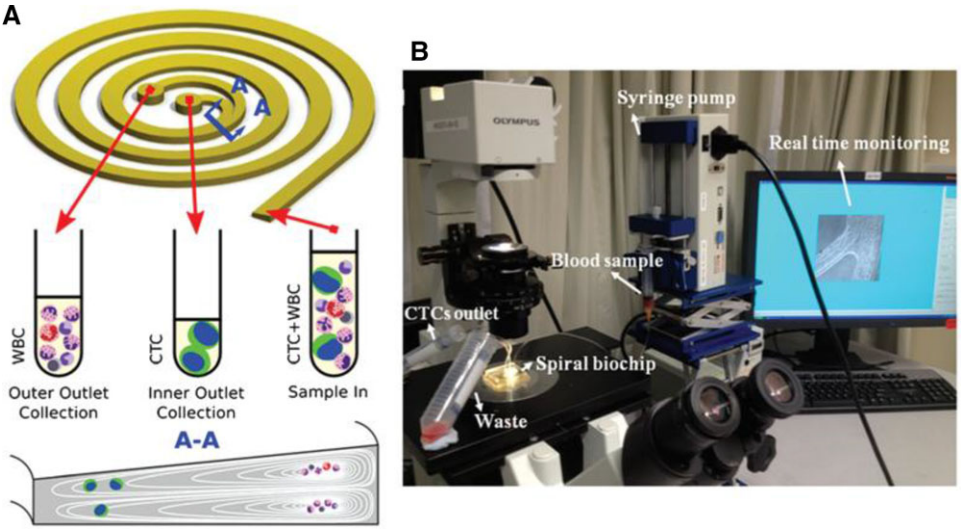

Figure 16. The designed device in reference [101]. Published by the Royal Society of Chemistry. https://creativecommons.org/licenses/by-nc/3.0/

at the outlet. While white blood cells and platelets are trapped inside the core. The lysed blood is pumped through the spiral chip using syringe pump where CTCs are separated from other blood components. For the three cell lines of MCF-7, T24, and MDA-MB-231, the isolation efficiency is more than 80%.

4 Concluding remarks

This review gives an overview of the development of microfluidic techniques for tumor cell detection. Microfluidic technology has advantages of portability, simplicity, label free, and low cost. A variety of microfluidics technologies for breast, colorectal, and prostate cancer cells detection is described and evaluated, showing their huge potential in point-of-care diagnosis.

The methods of microfluidic technology for CTCs detection can be summarized as active method and passive method. Both of the two methods can obtain ideal detection results, but have different emphases on the study. For active methods, they lay the emphases on the study of isolating cells by extra forces, such as stretching cells by laser beams [30] testing the electrical pulses induced by cells [54], labeling cells by magnetic particles [75], and controlling cells in certain places by ultrasound [81]. However, extra forces have different impacts on tumor and normal cells due to their different chemical and physical properties. For passive methods there are no extra forces, tumor cells are isolated by their inherent characters [92] and by the forces induced from the flow [93]. Therefore, passive methods put the emphases of study on the design of microfluidic structure. Mostly, cells are isolated by their sizes. Therefore the device usually includes microsieve, pillar, or weir [83, 91]. It works as a filter that can filter out undesirable cells. If it takes advantage of flow force to control cells, there will be some micro channels with specialized structure [98, 101].

The comparison on working performances of the two methods can be figured out from Table 2. Flow rate of active method is relatively slower due to the fact that it needs more time for physical reaction. Cell viabilities are almost the same, both between 70∼90% according to the published data. But cell recovery efficiencies are varied. Active method can obtain the better results and the highest recovery efficiency reached 96%. This is because there is at least one more force added in a certain active method, it is easier to control cells.

However, there is still much room for improvement in this research field. First of all, most of the microfluidic devices are not fully integrated in this stage. They can isolate cells inside only with the help of traditional equipment. For instance, the device in reference [54] used a syringe pump to perfuse the sample and an amplifier to measure electrical current. Therefore the levels of versatility and integration of microfluidic chips for CTCs detection remains to be raised. Meanwhile, with the rapid growth of the healthcare market, more functions of microfluidic chips can be developed besides CTCs detection. Such as blood triglyceride monitoring [102], diabete ketosis identification [103], blood Cholesterol monitoring [104] and some other blood parameters monitoring [105–107]. Furthermore, such functional microfluidic chip can also be integrated with smartphone [105]. It can be seen as a family doctor, and can access the related biomedical information of the patient and give the precise, personalized healthcare consults. There already have some researches about smartphone-based microfluidic systems at the point of care [108]. Such as imaging and measuring the DNA molecules [109], and monitoring uric acid and glucose [106, 107]. According to this idea, we could foresee that the CTCs detection can also be integrated in a smartphone, even be remote controlled [110].

Another deficiency is the sample pretreatment. Human blood sample has high concentration and variety of cells, which leads to complex stress on cells and increased intercellular interference. Therefore, it is hard to isolate target cells from blood directly. Samples need to be diluted and

pretreated, and this takes a lot of time and make the process complicate. It is important to keep studying on this point and find a better solution. However, there is a tradeoff between accuracy, throughput, and complexity in microfluidic chips design. Though this review, it is wish to attract more research interests in microfluidic techniques in tumor cell detection and promote medical technology.

This work is supported by the Talent Introduction Project of Chengdu University of Information Technology under Grant KYTZ201818, and China Scholarship Council under award number 201808515091.

The authors have declared no conflict of interest.

5 References

[1] Biral, A., Zordan, D., Zanella, A., *IEEE Trans. Mol. Biol. Multi-Scale Commun.* 2016, *1*, 122–134.

[2] Pantel, K., Alix-Panabières, C., *Trends Mol. Med.* 2010, *16*, 398–406.

[3] Williams, S. C., *Cancer Biol. Ther.* 2013, *110*, 4861–4861.

[4] Cima, I., Yee, C. W., Iliescu, F. S., Phyo, W. M., Lim, K. H., Lliescu, C., Tan, M. H., *Biomicrofluidics* 2013, *7*, 457–461.

[5] Marx V., *Nature* 2013, *494*, 133–136.

[6] Lianidou, E. S., Markou, A., *Clin. Chem.* 2011, *57*, 1242–1255.

[7] Zhe, X., Cher, M. L., Bonfil, R. D., *Am. J. Cancer Res.* 2011, *1*, 740–751.

[8] Guo, J., Pui, T. S., Ban, Y. L., Rahman, A. R. A., Kang, Y., *IEEE Trans. Biomed. Eng.* 2013, *60*, 3269–3275.

[9] Xia, J., Chen, X., Zhou, C. Z., Li, Y. G., Peng, Z. H., *IET Nanobiotechnol.* 2011, *5*, 114–120.

[10] Chin, C. D., Linder, V., Sia, S. K., *Lab Chip* 2006, *7*, 41–57.

[11] Hadd, A. G., Raymond, D. E., Halliwell, J. W., Jacobson, S. C., Ramsey, J. M., *Anal. Chem.* 1997, *69*, 3407–3412.

[12] Harrison, D. J., Fluri, K., Seiler, K., Fan, Z. H., Effenhauser, C. S., Manz, A., *Science* 1993, *261*, 895–897.

[13] Fluri, K., Fitzpatrick, G., Chiem, N., Harrison, D. J., *Anal. Chem.* 1996, *68*, 4285–4290.

[14] Daw, R., Finkelstein, J., *Nature* 2006, *442*, 367–367.

[15] Yager, P., Edwards, T., Fu, E., Helton, K., Nelson, K., Tam, M. R., Weigl, B. H., *Nature* 2006, *442*, 412–418.

[16] Zhang, C., Xing, D., *Anal. Chem.* 2010, *110*, 4910–4947.

[17] Martin, L., Meier, M., Lyons, S. M., Sit, R. V., Marzluff, W. F., Quake, S. R., Chang, H. Y., *Nat. Methods* 2012, *9*, 1192–1194.

[18] Yin, H., Marshall, D., *Curr. Opin. Biotechnol.* 2012, *23*, 110–119.

[19] Junkin, M., Tay, S., *Lab Chip* 2014, *14*, 1246–1260.

[20] Huh, D., Hamilton, G. A., *Trends Cell Biol.* 2011, *21*, 745–754.

[21] Huh, D., Matthews, B. D., Mammoto, A., Montoya-Zavala, M., Hsin, H. Y., Ingber, D. E., *Science* 2010, *328*, 1662–1668.

[22] Marx, U., Walles, H., Hoffmann, S., Lindner, G., Horland, R., Sonntag, F., Klotzbach, U., Sakharov, D., Tonevitsky, A., Lauster, R., *ATLA-Altern. Lab. Anim.* 2012, *40*, 235–257.

[23] Ma, W., Zeng, R. H., Liu, D. Y., Zohar, Y., Lee, K., *The 9th IEEE International Conference on Nano/Micro Engineered and Molecular Systems*, Hawaii, USA, April 2014, pp. 333–336.

[24] Gupta, G. P., Massagué, J., *J. Clin. Invest.* 2004, *114*, 1691–1693.

[25] Wittekind, C., Neid, M., *Oncology* 2005, *69*, 14–16.

[26] Howard, D. J., Seo, Y. J., Hahm, B., Kwon, J. W., *IEEE Sens. J.* 2014, *14*, 5–6.

[27] Nagrath, S., Sequist, L. V., Maheswaran, S., Bell, D. W., Irimia, D., Ulkus, L., Smith, M. R., Kwak, E. L., Digumarthy, S., Muzikansky, A., *Nature* 2007, *450*, 1235–1239.

[28] Guo, J., Chen, Z., Ban, Y. L., Kang, Y. J., *IEEE Trans. Emerg. Top. Comput.* 2017, *5*, 518–525.

[29] Macdonald, M. P., Spalding, G. C., Dholakia, K., *Nature* 2003, *426*, 421–424.

[30] Guck, J., Schinkinger, S., Lincoln, B., Wottawah, F., Ebert, S., Romeyke, M., Lenz, D., Erickson, H. M., Ananthakrishnan, R., Mitchell, D., *Biophys. J.* 2005, *88*, 3689–3698.

[31] Guo, J. H., Ma, X., Menon, N. V., Li, C. M., Zhao, Y. L., Kang, Y. J., *IEEE J. Sel. Top. Quantum Electron.* 2015, *21*, 392–398.

[32] Hu, X. Y., Bessette P. H., Qian J. R., Meinhart, C. D., Daugherty, P. S., Soh, H. T., *Proc. Natl. Acad. Sci. USA* 2005, *102*, 15757–15761.

[33] Vahey, M. D., Voldman, J., *Anal. Chem.* 2008, *80*, 3135–3143.

[34] Robert, D., Pamme, N., Conjeaud, H., Gazeau, F., Iles, A., Wilhelm, C., *Lab Chip* 2011, *11*, 1902–1910.

[35] Xia, N., Hunt, T. P., Mayers, B. T., Alsberg, E., Whitesides, G. M., Westervelt, R. M., Ingber, D. E., *Biomed. Microdevices* 2006, *8*, 299–308.

[36] Shi, J. J., Huang, H., Stratton, Z., Huang, Y. P., Huang, T. J., *Lab Chip* 2009, *9*, 3354–3359.

[37] Petersson, F., Aberg, L., Swärdnilsson, A. M., Laurell, T., *Anal. Chem.* 2007, *79*, 5117–5123.

[38] Liu, Y., Hartono, D., Lim, K. M., *Biomicrofluidics* 2012, *6*, 012802.

[39] Norris, J. V., Evander, M., Horsmanhall, K. M., Nilsson, J., Laurell, T., Landers, J. P., *Anal. Chem.* 2009, *81*, 6089–6095.

[40] Zhang, H., Liu, K. K., *J. R. Soc. Interface* 2008, *5*, 671–690.

[41] Wei, M. T., Karmenyan, A., Chiou, A., *2005 Pacific Conference on Lasers and Electro-Optics*, Sydney, Australia 2005, pp. 1098–1099.

[42] Guck, J, Ananthakrishnan, R., Mahmood, H., Moon, T. J., Cummingham, C. C., Kas, J., *Biophys. J.* 2001, *81*, 767–784.

[43] Guo, J. H., Liu, X. H., Kang, K., Ai, Y., Wang, Z. M., Kang, Y. J., *J. Lightwave Technol.* 2015, *33*, 3433–3438.

[44] Asghar, W., Wan, Y., Ilyas, A., Bachoo, R., Kim, Y. T., Iqbal, S. M., *Lab Chip* 2012, *12*, 2345–2352.

[45] Gou, J. H., Pui, T. S., Ban, Y. L., Rahman, A. R. A., Kang, Y., *IEEE Trans. Biomed. Eng.* 2013, *60*, 3269–3275.

[46] Gattu, S., Crihfield, C. L., Lu, G., Bwanali, L., Veltri, L. M., Holland, L. A., *Methods* 2018, *146*, 93–106.

[47] Chan, P. C., Chen, Y., Randell, E. W., *Clin. Biochem.* 2018, *51*, 29–37.

[48] Foret, F., Kutter, J., Oleksandrov, S., Aman, A., Lim, W., Kim, Y., Bae, N. H., Lee, K. G., Lee, S. J., Park, S., *Electrophoresis* 2018, *39*, 456–461.

[49] Kasicka V., *Electrophoresis* 2018, *39*, 209–234.

[50] Park, J., Jo, K. H., Park, H. Y., Hahn, J. H., *Sens. Actuator B* 2016, *232*, 428–433.

[51] Yan, X. X., Liu, W. F., Yuan, Y., Chen, C. P., *Anal. Methods* 2015, *7*, 5295–5302.

[52] Smolka, M., Puchberger-Enengl, D., Bipoun, M., Klasa, A., Kiczkajlo, M., Smiechowski, W., Sowinski, P., Krutzler, C., Keplinger, F., Vellekoop, M. J., *Precis. Agric.* 2016, *18*, 152–168.

[53] Zhang, X. F., Chu, H. K., Zhang, Y., Bai, G. H., Wang, K. Q., Tan, Q. L., Sun, D., *J. Micromech. Microeng.* 2015, *25*, 105004.

[54] Guo, J. H., Chen, Z., Ban, Y. L., Kang, Y. J., *IEEE Trans. Emerg. Top. Comput.* 2017, *5*, 518–525.

[55] Xu, W. W., Mezencev, R., Kim, B., Wang, L. J., McDonald, J., Sulchek, T., *PloS One* 2012, *7*, e46609.

[56] Byun, S., Son, S., Amodei, D., Cermak, N., Shaw, J., Kang, J. H., Hecht, V. C., Winslow, M. M., Jacks, T., Mallick, P., *Proc. Natl. Acad. Sci. USA* 2013, *110*, 7580–7585.

[57] Guo, J. H., Huang, X. W., Ai Y., *Anal. Chem.* 2015, *87*, 6516–6519.

[58] Becker, F. F., Wang, X. B., Huang, Y., Pethig, R., Vykoukal, J., Gascoyne, P. R. C., *Proc. Natl. Acad. Sci. USA* 1995, *92*, 860–864.

[59] Nguyen, N. V., Jen, C. P., *Biosens. Bioelectron.* 2018, *121*, 10–18.

[60] Yang, F., Yang, X. M., Jiang, H., Bulkhaults, P., Wood, P., Hrushesky, W., Wang, G. R., *Biomicrofluidics* 2010, *4*, 13204.

[61] Gupta, V., Jafferji, I., Garza, M., Melnikova, V. O., Hasegawa, D. K., Pethig, R., Davis, D. W., *Biomicrofluidics* 2012, *6*, 024133.

[62] Jen, C. P., Chang, H. H., *Biomicrofluidics* 2011, *5*, 034101.

[63] Wang, J., Pumera, M., Chatrathi, M. P., Esccarpa, A., Konrad, R., Griebel, A., Dorner, W., Lowe, H., *Electrophoresis* 2015, *23*, 596–601.

[64] Moon, H. S., Kwon, K., Kim, S. I., Han, H., Sohn, J., Lee, S., Jung, H. I., *Lab Chip* 2011, *11*, 1118–1125.

[65] Cummings, E. B., Singh, A. K., *Anal. Chem.* 2003, *75*, 4724–4731.

[66] Chou, C. F., Tegenfeldt, J. O., Bakajin, O., Chan, S. S., Cox, E. C., Darnton, N., Duke, T., Austin, R. H., *Biophys. J.* 2002, *83*, 2170–2179.

[67] Salmanzadeh, A., Kittur, H., Sano, M. B., Roberts, P. C., Schmelz, E. M., Davalos, R. V., *Biomicrofluidics* 2012, *6*, 024104.

[68] Sano, M. B., Caldwell, J. L., Davalos, R. V., *Biosens. Bioelectron.* 2011, *30*, 13–20.

[69] Lu, K. Y., Wo, A. M., Lo, Y. J., Chen, K. C., Lin, C. M., Yang, C. R., *Biosens. Bioelectron.* 2006, *22*, 568–574.

[70] Brown, R. B., Audet, J., *J. R. Soc. Interface* 2008, *5*, S131–S138.

[71] Xia, N., Hunt, T. P., Mayers, B. T., Alsberg, E., Whitesides, G. M., Westervelt, R. M., *Ingber, DE, Biomed. Microdevices* 2006, *8*, 299–308.

[72] Berger, M., Castelino, J., Huang, R., Shah, M., Austin, R. H., *Electrophoresis* 2001, *22*, 3883–3892.

[73] Han, K. H., Frazier, A. B., *Lab Chip* 2006, *6*, 265–273.

[74] Inglis, D. W., Riehn, R., Austin, R. H., Sturm, J. C., *Appl. Phys. Lett.* 2004, *85*, 5093–5095.

[75] Mohamadi, R. M., Besant, J. D., Mepham, A., Green, B., Mahmoudian, L., Gibbs, T., Lvanov, I., Malvea, A., Stojocic, J., Allan, A. L., *Angew. Chem. Int. Ed.* 2015, *54*, 139–143.

[76] Coumans, F. A. W., van Dalum, G., Beck, M., Terstappen, L. W. M. M., *PLoS One* 2013, *8*, e61774.

[77] Kim, S. H., Antfolk, M., Kobayashi, M., Kaneda, S., Laurell, T., Fujii, T., *Lab Chip* 2015, *15*, 4356–4363.

[78] Dykes, J., Lenshof, A., Åstrand-Grundström, I. B., Laurell, T., Scheding, S., *PLoS One* 2011, *6*, e23074.

[79] Yang, A. H., Soh, H. T., *Anal. Chem.* 2012, *84*, 10756–10762.

[80] Faridi, M. A., Ramachandraiah, H., Iranmanesh, I., Grishenkov, D., Wiklund, M., Russom, A., *Biomed. Microdevices* 2017, *19*, 23.

[81] Antfolk, M., Kim, S. H., Koizumi, S., Fujii, T., Laurell, T., *Sci Rep.* 2017, *7*, 46507.

[82] Cho, H., Kim, J., Song, H., Sohn, K. Y., Jeon, M., Han, K. H., *Analyst* 2018, *143*, 2936–2970.

[83] Huang, L. R., Cox, E. C., Austin, R. H., Sturm, J. C., *Science* 2004, *304*, 987–990.

[84] Prentki, P., Krisch, H. M., *Gene* 1984, *29*, 303–313.

[85] Domian, I. J., Quon, K. C., Shapiro, L., *Cell* 1997, *90*, 415–424.

[86] Yusa, A., Toneri, M., Masuda, T., Ito, S., Yamamoto, S., Okochi, M., Kondo, N., Iwata, H., Yatabe, Y., Ichinosawa, Y., *PLoS One* 2014, *9*, e88821.

[87] Lim, L. S., Hu, M., Huang, M. C., Cheong, W. C., Gan, A. T. L., Looi, X. L., Leong, S. M., Koay, E. S. C., Li, M. H., *Lab Chip* 2012, *12*, 4388–4396.

[88] Hosokawa, M., Hayata, T., Fududa, Y., Arakaki, A., Yoshino, T., Tanaka, T., Matsunaga, T., *Anal. Chem.* 2010, *82*, 6629–6635.

[89] Tang, Y. D., Shi, J., Li, S. S., Wang, L., Cayre, Y. E., Chen, Y., *Sci Rep.* 2016, *4*, 6052.

[90] Gleghorn, J. P., Pratt, E. D., Denning, D., Liu, H., Bander, N. H., Tagawa, S. T., Nanus, D. M., Giannakakou, P. A., Kirby, B. J., *Lab Chip* 2010, *10*, 27–29.

[91] Zhou, M. D., Hao, S. J., Williams, A. J., Harouaka, R. A., Schrand, B., Rawal, S., Ao, Z., Brenneman, R., Gilboa, E., Lu, B., *Sci Rep.* 2015, *5*, 7967–7977.

[92] Bu, J., Kang, Y. T., Lee, Y. S., Kim, J., Cho, Y. H., Moon, B. I., *Biosens. Bioelectron.* 2017, *91*, 747–755.

[93] Martel, J. M., Toner, M., *Annu. Rev. Biomed. Eng.* 2014, *16*, 371–396.

[94] Segre, G., Silberberg, A., *J. Fluid Mech.* 2006, *14*, 136–157.

[95] Segre, G., Silberberg, A., *J. Fluid Mech.* 1962, *14*, 115–135.

[96] Matas, J. P., Morris, J. F., Guazzelli, E., *Phys. Rev. Lett.* 2003, *90*, 014501.

[97] Choi, Y. S., Lee, S. J., *Microfluid. Nanofluid.* 2010, *9*, 819–829.

[98] Zhou, J., Giridhar, P. V., Kasper, S., Papautsky, I., *Lab Chip* 2013, *13*, 1919–1929.

[99] Di Carlo, D., *Lab Chip* 2009, *9*, 3038–3046.

[100] Kuntaegowdanahalli, S. S., Bhagat, A. A., Kumar, G., Papautsky, I., *Lab Chip* 2009, *9*, 2973–2980.

[101] Warkiani, M. E., Guan, G., Luan, K. B., Lee, W. C., Bhagat, A. A. S., Chaudhuri, P. K., Tan, D. S. W., Lim, W. T., Lee, S. C., Chen, P. C. Y., *Lab Chip* 2014, *14*, 128–137.

[102] Wang, J., Huang, X., Tang, S., Shi, G., Ma, X., Guo, J., *IEEE J. Biomed. Health Inform.* 2018. https://doi.org/10.1109/JBHI.2018.2845860.

[103] Gou, J. H., Huang, X., Ma, X., *Sens. Actuator B* 2018, *275*, 446–450.

[104] Fu, Y. S., Guo, J. H., *IEEE Trans. Biomed. Circuits Syst.* 2018, *12*, 784–790.

[105] Guo, J. H., *IEEE Trans. Ind. Inform.* 2018, *14*, 2592–2597.

[106] Guo, J. H., Ma, X., *Biosens. Bioelectron.* 2017, *94*, 415–419.

[107] Guo, J. H., *Anal. Chem.* 2016, *88*, 11986–11989.

[108] Xu, D. D., Huang, X. W., Guo, J. H., Ma, X., *Biosens. Bioelectron.* 2018, *110*, 78–88.

[109] Wei, Q. S., Luo, W., Chiang, S., Kappel, T., Mejia, C., Tseng, D., Chan, R. Y. L., Yan, E., Qi, H. F., Shabbir, F., *ACS Nano* 2014, *8*, 12725–12733.

[110] Xu, J., Jian, X. D., Wang, L., Shen, Y. F., Yuan, K. F., Nie, Y., Tian, Y. X., Ma, X., Guo, J. H., *IEEE Trans. Ind. Inform.* 2018, https://doi.org/10.1109/TII.2018.2879430.

